Electronic-band parameters in strained $Si_{1-x}Ge_x$ alloys on $Si_{1-y}Ge_y$ substrates

Martin M. Rieger and P. Vogl
Physik Department and Walter Schottky Institut, Technische Universität München, D-85747 Garching, Germany
(Received 14 September 1992; revised manuscript received 3 May 1993)

A systematic theoretical study of the electronic properties of pseudomorphic (100)-strained $Si_{1-x}Ge_x$ alloys grown on unstrained $Si_{1-y}Ge_y$ substrates is presented. Based on nonlocal empirical pseudopotential calculations with spin-orbit interactions, realistic estimates of the conduction- and valence-band-edge energies, higher-energy-band minima, effective masses, deformation potentials, and heterostructure band offsets for the whole range of alloy compositions x and y and strain are presented. The theory predicts that the band edges of weakly stressed Ge fall within the wider gap of the $Si_{1-y}Ge_y$ substrate for $0.7 < y < 1$ (type-I alignment), in contrast to any Si-rich combination of active layer and substrate.

I. INTRODUCTION

The successful fabrication of Si/Ge strained layer superlattices and multiple-quantum-well systems has opened the prospect to fabricate both optoelectronic and electronic devices using the highly advanced Si technology. Through the advent of molecular-beam epitaxy, the properties of the SiGe system can be varied substantially in a controlled fashion. By selecting proper amounts of strain, number, and type of Si/Ge layers, alloy compositions, or growth directions, exciting new properties that drastically differ from pure Si have been demonstrated experimentally in strained-layer superlattices[1-3] and in heterostructures.[4-6] These experiments have been complemented by extensive theoretical studies of band alignments[7-9] and optical properties[10-13] of strained layer superlattices.

In most Si/Ge devices such as modulation-doped field-effect transistors, the electrically active material is a (100)-strained lattice-matched $Si_{1-x}Ge_x$ layer that is either grown on top of a thick $Si_{1-y}Ge_y$ substrate or is embedded in between such substrates that determine the lateral lattice constant and consequently the strain. In the regime of high electric fields that is relevant for all submicrometer devices, the electron and hole distribution functions depend critically on the alloy and strain dependence of the valley separation energies, minimum and higher band gaps, deformation potentials, and the heterostructure band offsets.

The energy gaps and masses that are relevant for transport applications are still only crudely known as a function of x and y in strained $Si_{1-x}Ge_x$:$Si_{1-y}Ge_y$ alloys. First insights into the interplay of strain and alloying in these materials were given by Abstreiter and coworkers[14,15] and by People.[16] More recently, $\mathbf{k}\cdot\mathbf{p}$ calculations of optical properties[17] and Monte Carlo calculations of the hole transport[18] were performed for strained Si on $Si_{1-y}Ge_y$, using Si and Ge averages for the $\mathbf{k}\cdot\mathbf{p}$ parameters. Empirical tight-binding calculations in strained SiGe alloys have allowed valuable qualitative insight into symmetry-related properties;[19] however, conduction bands and their masses can be accurately modeled in this approach only if a very large number of fitting parameters is introduced.[20] Pseudopotential calculations of the parabolic hole masses were done by Gell for lattice-matched Ge on $Si_{1-y}Ge_y$.[21]

The main goal of this paper is to provide a consistent and complete set of band parameters that are needed for quantitative transport calculations in SiGe alloys. Specifically, this paper presents realistic estimates of several conduction- and valence-band-edge energies, effective masses, deformation potentials, and heterostructure band offsets for the whole range of alloy compositions and strain in the lattice matched (100)-strained $Si_{1-x}Ge_x$:$Si_{1-y}Ge_y$ system. The calculations are performed in the framework of the empirical nonlocal, relativistic pseudopotential theory. We derive explicit expressions for the effective-mass tensors for electrons in terms of the nonlocal pseudopotentials and Bloch functions, employing $\mathbf{k}\cdot\mathbf{p}$ theory. Within the rigid-ion approximation, explicit expressions are also given for relative strain deformation potentials.

The paper is organized as follows. The pseudopotential Hamiltonian is defined in Sec. II. We have determined the various mass parameters of the conduction and valence band by means of a nonlocal variant of the $\mathbf{k}\cdot\mathbf{p}$ method. In Sec. III, explicit expressions for the conduction- and valence-band masses and deformation potentials are given. The numerical results for the energy gaps, effective masses, deformation potentials, and band offsets are summarized in Sec. IV and the major findings concisely summed up in Sec. V.

II. THE EMPIRICAL PSEUDOPOTENTIAL METHOD

Ideally, one would like to calculate electronic band parameters with *ab initio* methods such as the local-density functional schemes. While these methods are quite accurate for ground-state properties and some excitation energies,[22] they still do not meet the accuracy needed for transport parameters. Ge, for example, is found to be a metal[22] in the framework of local-density theory. While quasiparticle band structures are generally more satisfactory,[22] recent calculations of this type still predict Ge to possess a direct and underestimated[23] or even almost vanishing[24] energy gap. Consequently one is forced to intro-

duce some empirical element in the calculation. Here we will employ the empirical pseudopotential approach in its nonlocal relativistic version as developed by Chelikowsky and Cohen.[25] This method is known to reproduce with fair accuracy many electronic-structure properties of semiconductors including the principal energy gaps, electron-phonon matrix elements, and optical response functions.[25,26]

We solve the electronic Schrödinger equation with the pseudo-Hamiltonian

$$H=-\frac{\hbar^2}{2m}\Delta+V_{\rm loc}+V_{\rm nloc}+V_{\rm so} , \tag{1}$$

which is represented in a plane-wave basis $|\mathbf{K}\sigma\rangle=|\exp\{i(\mathbf{k}+\mathbf{G})\cdot\mathbf{r}\}\rangle|\sigma\rangle$ with $\mathbf{K}=\mathbf{k}+\mathbf{G}$ and spin states $|\sigma\rangle$. Here $\mathbf{k}$ is the reduced wave vector and the $\mathbf{G}$ are reciprocal lattice vectors. In Eq. (1), $V_{\rm loc}(\mathbf{r})$ is the local pseudopotential operator of the crystal and is here assumed to consist of a superposition of spherical, screened, local atomic pseudopotentials $V(\mathbf{r})$ of one atomic species. This leads to the Fourier representation

$$V_{\rm loc}(\mathbf{G})=S(\mathbf{G})V_{\rm loc}^{\rm atom}(|\mathbf{G}|) , \tag{2}$$

where

$$V_{\rm loc}^{\rm atom}(\mathbf{G})=\frac{1}{\Omega_{\rm cell}}\int d\mathbf{r}\, V_{\rm loc}^{\rm atom}(\mathbf{r})\exp(-i\mathbf{G}\cdot\mathbf{r}) \tag{3}$$

is normalized to the primitive unit $\Omega_{\rm cell}$ and the structure factor $S(\mathbf{G})$ contains a sum over the N_α atomic positions $\mathbf{x}_\alpha$ in the primitive cell,

$$S(\mathbf{G})=\frac{1}{N_\alpha}\sum_\alpha \exp(-i\mathbf{G}\cdot\mathbf{x}_\alpha) . \tag{4}$$

Analogously, Eq. (1) includes a nonlocal, angular-momentum-dependent pseudopotential,

$$V_{\rm nloc}(\mathbf{K},\mathbf{K}')=S(\mathbf{K}-\mathbf{K}')V_{\rm nloc}^{\rm atom}(\mathbf{K},\mathbf{K}') . \tag{5}$$

With $\hat{P}_l$ denoting the angular momentum projector, the nonlocal part of the atomic potential is written as

$$V_{\rm nloc}^{\rm atom}(\mathbf{r})=\sum_l A_l f_l(r)\hat{P}_l ,$$
$$f_l(r)=\begin{cases}\Theta(R_l-r) & \text{in Si}\\ \exp(-r^2/R_l^2) & \text{in Ge} .\end{cases} \tag{6}$$

Following Ref. 25, the core form factor $f_l(r)$ is represented by a Heaviside step function [$\Theta(x)=1$ for $x\geq 0$ and 0 otherwise) in Si and by a Gaussian function in Ge. For Si only the $l=0$ contribution whereas for Ge only the $l=2$ contribution is included explicitly in Eq. (6). The spin-orbit interaction

$$V_{\rm so}=\sum_l V_{l,{\rm so}}\mathbf{L}\cdot\mathbf{S}\hat{P}_l \tag{7}$$

is taken into account only for Ge (and the $Si_{1-x}Ge_x$ alloys, see below) and only the dominant $l=1$ core states are included in Eq. (7). In a plane-wave basis, Eq. (7) has the form

$$V_{\rm so}(\mathbf{K}\sigma,\mathbf{K}'\sigma')=-\frac{2i\mu}{\hbar}\left[\frac{(\Omega_{\rm cell}/2)^{1/3}}{\pi}\right]^2 \times S(\mathbf{K}-\mathbf{K}')B(K)B(K') \times\mathbf{K}\times\mathbf{K}'\cdot\langle\sigma|\mathbf{S}|\sigma'\rangle , \tag{8}$$
$$B(K)=\frac{5-(K/\zeta)^2}{5[1+(K/\zeta)^2]^4} ,$$

where we have used an analytical representation for the overlap integrals $B(K)$.[25,27] All pseudopotential parameters are summarized in Table I and basically agree with those of Ref. 25. In Ge, only the spin-orbit parameter μ has been slightly adjusted to account for the differences in $B(K)$, but for Si we dropped the energy dependence of the weight factors $A_l(E)$ in the nonlocal part of the pseudopotential altogether, since the expression for $A_l(E)$ in Ref. 25 [Eq. (11) in their paper], taken as a function of $\mathbf{k}$, has discontinuous second-order partial derivatives. Even though this effect is small, it translates into undefined masses of the energy bands at $\mathbf{k}=\mathbf{0}$. We have therefore slightly readjusted the remaining potential parameters so as to reproduce as closely as possible the previous results of Ref. 25.

This paper focuses on the properties of (100)-tetragonally distorted $Si_{1-x}Ge_x$ alloys with a lateral lattice constant $a_\parallel(x)$ equal to the bulk lattice constant $a_0(y)$ of an unstrained substrate $Si_{1-y}Ge_y$ alloy that has a different composition y. The strained $Si_{1-x}Ge_x$ layer is considered thick enough to exhibit bulk properties. The lattice constant $a_\perp(x)$ of the strained alloy in the direction perpendicular to the interface is adapted so as to minimize the elastic energy,[1]

$$a_\perp(x)=a_0(x)\left[1-2\frac{c_{12}(x)}{c_{11}(x)}\frac{a_\parallel(x)-a_0(x)}{a_0(x)}\right] , \tag{9}$$

where c_{11} and c_{12} are the elastic constants. For pure Si (Ge), we have used $c_{11}=1.675$ (1.315) Mbar and $c_{12}=0.650$ (0.494) Mbar,[28] and linearly interpolated these constants for the alloy.

A biaxially strained $Si_{1-x}Ge_x$ crystal has a face-centered tetragonal lattice. Consequently, the six X points in the Brillouin zone split into four X points and two Z points. Correspondingly, there are four $\Delta_\parallel$ and

TABLE I. The pseudopotential parameters used in this work. All parameters are in rydbergs, except where specified otherwise.

Parameter	Ge	Si
$V(\sqrt{3})$	−0.221	−0.2241
$V(\sqrt{8})$	0.019	0.0520
$V(\sqrt{11})$	0.056	0.0724
A_0	0	0.03
A_2	0.275	0
R_l (Å)	1.22	1.06
μ	0.000 965	0
ζ (Å^{-1})	10.091 1	0

two $\Delta_\perp$ axes. The four L points remain equivalent and are conventionally labeled by N in a tetragonal lattice.

The alloys are treated in the virtual-crystal approximation by linearly interpolating the form factors of the individual constituents. The lattice constants for the bulk $Si_{1-x}Ge_x$ alloys are measured values from Ref. 29, which can be represented in the form

$$a_0(x)=a_0(\mathrm{Si})+0.200\,326x(1-x)+[a_0(\mathrm{Ge})-a_0(\mathrm{Si})]x^2 . \quad (10)$$

The pseudopotential calculations in the strained crystal are performed by invoking the rigid-ion approximation. This implies two modifications in the pseudopotentials. First, the normalizing volume changes with the strained unit cell volume. Second, the local pseudopotential form factors enter the calculation at the strained reciprocal lattice vectors. These values have been obtained by performing a cubic spline interpolation through the atomic pseudopotential form factors, $V(0)=-2E_F/3$, $V(\sqrt{3})$, $V(\sqrt{8})$, $V(\sqrt{11})$, and $V(3k_F)=0$, where E_F and k_F are the Fermi energy and wave vector of the free-electron gas appropriate to the electron density in the cubic crystal. We have included about 180 plane waves in the diagonalization of the Hamiltonian matrix which gives results converged to within approximately 1 meV.

III. k·p EXPRESSIONS FOR BAND PARAMETERS

A. Conduction-band masses in strained alloys

The conductivity mass tensor $\mathbf{M}_{\mathrm{cond}}$ for a nondegenerate band edge of energy E_c with N equivalent minima located at wave vectors $\mathbf{k}_\nu$ is given by

$$(\mathbf{M}_{\mathrm{cond}}^{-1})_{ij}=\frac{1}{N}\sum_{\nu}^{\text{valleys}}(\mathbf{M}_\nu^{-1})_{ij}=\frac{1}{N}\sum_{\nu}^{\text{valleys}}\frac{1}{\hbar^2}\frac{\partial^2}{\partial k_i\partial k_j}E_c(\mathbf{k}_\nu) \quad (11)$$

and determines the low field mobility. The most efficient and accurate method to calculate these effective masses is provided by the $\mathbf{k}\cdot\mathbf{p}$ theory, which will be employed in this paper.[30] As the pseudopotentials in Eqs. (6)–(8) are nonlocal, a few amendments to the conventional $\mathbf{k}\cdot\mathbf{p}$ theory, which assumes the commutability of $\exp(i\mathbf{k}\cdot\mathbf{r})$ and the potential operator, have to be added.[31] Let us assume a Hamiltonian

$$H=-\frac{p^2}{2m}+V_{\mathrm{loc}}(\mathbf{r})+U_{\mathrm{nloc}} , \quad (12)$$

where all nonlocal contributions such as Eqs. (6) and (7) have been lumped together into U_{nloc}. Furthermore, let the wave vector $\mathbf{k}$ and band index n correspond to a nondegenerate (or only Kramers's degenerate) band extremum associated with valley ν. By expanding the plane-wave representation

$$H(\mathbf{K}+\boldsymbol{\kappa},\mathbf{K}'+\boldsymbol{\kappa})=\frac{\hbar^2}{2m}|\mathbf{K}+\boldsymbol{\kappa}|^2\delta_{\mathbf{K}\mathbf{K}'}+V_{\mathrm{loc}}(\mathbf{K}-\mathbf{K}')+U_{\mathrm{nloc}}(\mathbf{K}+\boldsymbol{\kappa},\mathbf{K}'+\boldsymbol{\kappa}) , \quad (13)$$

with $\mathbf{K}=\mathbf{k}+\mathbf{G}$ and $\mathbf{K}'=\mathbf{k}+\mathbf{G}'$ to second order in the small wave vector $\boldsymbol{\kappa}$, one obtains the following expressions for the inverse effective-mass tensor:

$$(\mathbf{M}_\nu^{-1})_{ij}=\frac{1}{m}\delta_{ij}+\frac{1}{\hbar^2}\sum_{\mathbf{K}\mathbf{K}'}\langle n\mathbf{k}\sigma|\mathbf{K}\sigma\rangle\frac{\partial^2U_{\mathrm{nloc}}(\mathbf{K}\sigma,\mathbf{K}'\sigma)}{\partial k_i\partial k_j}\langle\mathbf{K}'\sigma|n\mathbf{k}\sigma\rangle+\frac{1}{m^2}\sum_{l\neq n,\sigma'}\frac{\langle n\mathbf{k}\sigma|\pi_i|l\mathbf{k}\sigma'\rangle\langle l\mathbf{k}\sigma'|\pi_j|n\mathbf{k}\sigma\rangle+\mathrm{c.c.}}{E_n(\mathbf{k})-E_l(\mathbf{k})} , \quad (14)$$

$$\langle n\mathbf{k}\sigma|\pi_i|l\mathbf{k}\sigma'\rangle=\sum_{\mathbf{K}\mathbf{K}'}\langle n\mathbf{k}\sigma|\mathbf{K}\sigma\rangle\pi_i(\mathbf{K}\sigma,\mathbf{K}'\sigma')\langle\mathbf{K}'\sigma'|l\mathbf{k}\sigma'\rangle , \quad (15)$$

$$\pi_i(\mathbf{K}\sigma,\mathbf{K}'\sigma')=\hbar K_i\delta_{\mathbf{K}\mathbf{K}'}\delta_{\sigma\sigma'}+\frac{m}{\hbar}\frac{\partial}{\partial k_i}U_{\mathrm{nloc}}(\mathbf{K}\sigma,\mathbf{K}'\sigma') .$$

In these equations, $\langle\mathbf{K}\sigma|n\mathbf{k}\sigma\rangle$ is the Fourier coefficient of the Bloch function solution $|n\mathbf{k}\sigma\rangle$ of Eq. (12). The terms proportional to U_{nloc} in Eqs. (14) and (15) represent corrections originating in the nonvanishing commutator of U_{nloc} with $\mathbf{r}$; we found these terms to contribute up to 20% to the calculated masses. Nevertheless, these corrections, as far as they contain nonlocal pseudopotential terms other than spin-orbit coupling, have not been taken into account in previous works.[32]

For a tetragonal strain, $\mathbf{M}_{\mathrm{cond}}$ is diagonal but contains two distinct elements $m_\parallel^{\mathrm{cond}}$ and $m_\perp^{\mathrm{cond}}$, determining the conductivity mass parallel and perpendicular to the interface plane. In contrast, the individual valley mass tensors can have three distinct elements when transformed to principal axes, namely a longitudinal mass m_l and two generally different transverse masses m_{t1} and m_{t2}. On the $\Delta_\parallel(N)$ axis, $m_{t2}(m_{t1})$ lies in the interface plane. The conduction-band minimum in strained $Si_{1-x}Ge_x$ alloys turns out to lie either on the $\Delta_\perp$ axis near $\mathbf{k}=(0,0,0.85)(2\pi/a_\perp)$, on the $\Delta_\parallel$ axis near $\mathbf{k}=(0.85,0,0)(2\pi/a_\parallel)$, or on the N point at $\mathbf{k}=(\pi/a_\perp,\pi/a_\parallel,\pi/a_\parallel)$. The explicit relation between the individual valley masses and the conductivity mass for these three situations is given by

$$\Delta_\perp:\ m_\parallel^{\mathrm{cond}}=m_t,\ m_\perp^{\mathrm{cond}}=m_l , \quad (16)$$

$$\Delta_{\parallel}: \quad \frac{1}{m_{\parallel}^{\text{cond}}}=\frac{1}{2}\left[\frac{1}{m_l}+\frac{1}{m_{t2}}\right], \quad m_{\perp}^{\text{cond}}=m_{t1} , \tag{17}$$

$$N: \quad \frac{1}{m_{\parallel}^{\text{cond}}}=\tfrac{1}{3}(1+\tfrac{2}{3}\varepsilon_{\text{ax}})\frac{1}{m_l}+\frac{1}{2m_{t1}}+\frac{1}{6}(1-\tfrac{4}{3}\varepsilon_{\text{ax}})\frac{1}{m_{t2}} ,$$

$$-\frac{1}{m_{\perp}^{\text{cond}}}=\tfrac{1}{3}(1-\tfrac{4}{3}\varepsilon_{\text{ax}})\frac{1}{m_l}+\frac{2}{3}(1+\tfrac{2}{3}\varepsilon_{\text{ax}})\frac{1}{m_{t2}} . \tag{18}$$

Only in the latter case does the conductivity mass depend explicitly on the amount of strain, in terms of the axial strain parameter $\varepsilon_{\text{ax}}=(a_{\perp}-a_{\parallel})/a_0$.

B. Valence-band parameters in unstrained alloys

In the conventional $\mathbf{k}\cdot\mathbf{p}$ approach, the valence-band parameters of tetrahedral semiconductors are defined for unstrained cubic materials and in the absence of spin-orbit interaction by taking the position that strain and spin-orbit effects are small and can be treated as additive perturbations.[30,33] Consequently, the Hamiltonian that *defines* the conventional valence-band $\mathbf{k}\cdot\mathbf{p}$ parameters is that of the *unstrained cubic* $Si_{1-x}Ge_x$ *alloy with the spin-orbit interaction set to zero,* i.e.,

$$H^{\text{cubic}}=-\frac{\hbar^2}{2m}\Delta+V_{\text{loc}}+V_{\text{nloc}} . \tag{19}$$

But we emphasize that all results for band gaps, effective masses, and band offsets presented in Sec. IV of this paper have been obtained by taking fully into account the strain and the spin-orbit interaction that are contained in the Hamiltonian Eq. (1).

In this section, we focus on the top of the valence bands at the Γ point in $Si_{1-x}Ge_x$ alloys. The $\mathbf{k}\cdot\mathbf{p}$ Hamiltonian for the three topmost valence bands in the form of Dresselhaus, Kip, and Kittel[33] is given by

$$H_v^{\text{cubic}}(\kappa)=\left[\frac{\hbar^2\kappa^2}{2m}\right]1+\frac{\hbar^2}{2m}\begin{bmatrix} L\kappa_x^2+M(\kappa_y^2+\kappa_z^2) & N\kappa_x\kappa_y & N\kappa_x\kappa_z \\ N\kappa_x\kappa_y & L\kappa_y^2+M(\kappa_x^2+\kappa_z^2) & N\kappa_y\kappa_z \\ N\kappa_x\kappa_z & N\kappa_y\kappa_z & L\kappa_z^2+M(\kappa_x^2+\kappa_y^2) \end{bmatrix} . \tag{20}$$

The eigenvalues of Eq. (20) are the heavy- and light-hole energies $E_v(\kappa)$, relative to the top of the valence band. In Ref. 33, the parameters L, M, and N have been defined in terms of the Bloch eigenfunctions associated with the three degenerate $\Gamma^{25'}$ valence-band states at $\mathbf{k}=0$ that transform as $|yz\rangle$, $|zx\rangle$, and $|xy\rangle$. Since the pseudopotential Hamiltonian Eq. (19) contains nonlocal potential contributions, we have to take care of corrections analogous to those in Eq. (14). Let us define the matrix $\mathbf{J}$ in Cartesian coordinates,

$$J_{ij}(\mathbf{G},\mathbf{G}')=(1-\tfrac{1}{2}\delta_{ij})\left\{\frac{\partial^2 V_{\text{nloc}}(\mathbf{K},\mathbf{K}')}{\partial k_i \partial k_j}\bigg|_{\mathbf{k}=0}+\frac{\hbar^2}{m^2}\sum_{n\neq v}\sum_{\mathbf{G}'',\mathbf{G}'''}\frac{\pi_i(\mathbf{G},\mathbf{G}'')\langle \mathbf{G}''|n\Gamma\rangle\langle n\Gamma|\mathbf{G}'''\rangle\pi_j(\mathbf{G}''',\mathbf{G}')+\text{c.p.}}{E_v(\Gamma)-E_n(\Gamma)}\right\} , \tag{21}$$

where

$$\pi(\mathbf{K},\mathbf{K}')=\hbar\mathbf{K}\delta_{\mathbf{K}\mathbf{K}'}+\frac{m}{\hbar}\nabla_{\mathbf{k}}V_{\text{nloc}}(\mathbf{K},\mathbf{K}') , \tag{22}$$

and c.p. stands for cyclic permutation of i and j. By applying a unitary transformation, the solutions of the Hamiltonian Eq. (19) associated with the $\Gamma^{25'}$ states can be transformed into states that transform as $|yz\rangle$, $|zx\rangle$, and $|xy\rangle$. In terms of these Bloch functions, the valence-band parameters L, M, and N are then found to be

$$L=\sum_{\mathbf{G}\mathbf{G}'}\langle yz|\mathbf{G}\rangle J_{xx}(\mathbf{G},\mathbf{G}')\langle \mathbf{G}'|yz\rangle ,$$

$$M=\sum_{\mathbf{G}\mathbf{G}'}\langle yz|\mathbf{G}\rangle J_{yy}(\mathbf{G},\mathbf{G}')\langle \mathbf{G}'|yz\rangle , \tag{23}$$

$$N=\sum_{\mathbf{G}\mathbf{G}'}\langle yz|\mathbf{G}\rangle J_{xy}(\mathbf{G},\mathbf{G}')\langle \mathbf{G}'|zx\rangle .$$

We have evaluated these expressions by summing over all bands (181 in this case) included in the Hamiltonian matrix at the Γ point.

C. Strain-deformation potentials

The strain deformation potentials as formulated by Bir and Pikus[30] are also defined in terms of the eigenstates of a cubic crystal Hamiltonian such as Eq. (19). In this section we write down the expressions for the conduction- and valence-band deformation potentials as valid for nonlocal pseudopotentials.

We assume that the wave vector $\mathbf{k}$ denotes an extremum of the conduction or valence bands. For a biaxial (100) strain, the symmetric strain tensor is

$$\hat{\varepsilon}=\begin{bmatrix} \varepsilon_{\parallel} & 0 & 0 \\ 0 & \varepsilon_{\parallel} & 0 \\ 0 & 0 & \varepsilon_{\perp} \end{bmatrix} , \tag{24}$$

where $\varepsilon_{\parallel}=(a_{\parallel}-a_0)/a_0$ and $\epsilon_{\perp}=(a_{\perp}-a_0)/a_0$. To first order in the strain, the band energies at $\mathbf{k}$ in the deformed crystal are the eigenvalues of the matrix[30]

$$H_{nn'}^{\varepsilon}(\mathbf{k})=\sum_{ij}\left\langle n\mathbf{k}\left|-\frac{p_i p_j}{m}+V_{ij}\right|n'\mathbf{k}\right\rangle\varepsilon_{ij}\equiv\sum_{ij}\Xi_{ij}(\mathbf{k})\varepsilon_{ij} , \tag{25}$$

$$V_{ij}=\{\partial V[(\mathbf{1}+\hat{\varepsilon})\mathbf{r}]/\partial\varepsilon_{ij}\}_{\hat{\varepsilon}=0} . \tag{26}$$

V is the pseudopotential in the strained crystal including both local and nonlocal parts and n,n' label a set of degenerate eigenstates. By assuming the ionic pseudopotential itself not to be affected by the strain (i.e., the rigid ion approximation), Eq. (25) can be evaluated explicitly. Using Eq. (2), the strained local crystal potential reads

$$V_{\rm loc}[(1+\hat{\varepsilon})\mathbf{r}]=\sum_{\mathbf{G}} S(\mathbf{G})\frac{\Omega_{\rm cell}}{\Omega^{\varepsilon}_{\rm cell}} V_{\rm loc}[(1-\hat{\varepsilon})\mathbf{G}]\exp(i\mathbf{G}\cdot\mathbf{r}) , \tag{27}$$

where $\Omega^{\varepsilon}_{\rm cell}$ is the strained cell volume and we have made use of the fact that $S(\mathbf{G})$ is invariant under strain. The nonlocal potential has an analogous form. We note that the strain dependence of the average crystal potential, i.e., the $\mathbf{G}=0$ term in Eq. (27), drops out in the interband deformation potentials that we solely focus on in this paper (Sec. IV). By expanding all potential terms to first order in the strain, one obtains

$$\begin{aligned}
\Xi_{ij}(\mathbf{k})&=\sum_{\mathbf{K}\mathbf{K}'}\langle n\mathbf{k}|\mathbf{K}\rangle\left[-\frac{\hbar^2}{m}K_iK_j\delta_{\mathbf{K}\mathbf{K}'}+V_{ij}(\mathbf{K},\mathbf{K}')\right]\\
&\quad\times\langle\mathbf{K}'|n'\mathbf{k}\rangle ,\\
V_{ij}(\mathbf{K},\mathbf{K}')&=V_{{\rm loc},ij}(\mathbf{K}-\mathbf{K}')+V_{{\rm nloc},ij}(\mathbf{K},\mathbf{K}') ,\\
V_{{\rm loc},ij}(\mathbf{G})&=-S(\mathbf{G})\left[\frac{G_iG_j}{|\mathbf{G}|}\frac{dV^{\rm atom}_{\rm loc}(q)}{dq}\bigg|_{q=G}\right]\\
&\quad-\delta_{ij}V_{\rm loc}(\mathbf{G}) ,\\
V_{{\rm nloc},ij}(\mathbf{K},\mathbf{K}')&=-S(\mathbf{K}-\mathbf{K}')\left\{K_j\frac{\partial}{\partial q_i}+K'_j\frac{\partial}{\partial q'_i}\right\}\\
&\quad\times V^{\rm atom}_{\rm nloc}(\mathbf{q},\mathbf{q}')|_{\mathbf{q}=\mathbf{K},\mathbf{q}'=\mathbf{K}'}\\
&\quad-\delta_{ij}V_{\rm nloc}(\mathbf{K},\mathbf{K}') .
\end{aligned} \tag{28}$$

In the following subsections, we consider separately the cases of nondegenerate and degenerate band edges.

1. Conduction-band deformation potentials

For nondegenerate conduction-band edges, the deformation potential tensor Ξ in Eq. (28) transforms in the same way as the effective-mass tensor, Eq. (14). Therefore, Ξ is diagonal along the Δ axis and has two independent components Ξ^{Δ}_l and Ξ^{Δ}_t. At the L point, there is only one independent component Ξ^{L} since the cubic axes are equivalent with respect to L.

In general, the strain-induced shift of a conduction-band edge δE_c has a hydrostatic and a traceless component. These shifts are conventionally expressed in terms of the potentials $\Xi_u=\Xi_l-\Xi_t$ and $\Xi_d=\Xi_t$ and are given by[30]

$$\begin{aligned}
\delta E_c(\Delta_\perp)&=(\Xi^{\Delta}_d+\tfrac{1}{3}\Xi^{\Delta}_u){\rm Tr}(\hat{\varepsilon})+\tfrac{2}{3}\Xi^{\Delta}_u(\varepsilon_\perp-\varepsilon_\parallel) ,\\
\delta E_c(\Delta_\parallel)&=(\Xi^{\Delta}_d+\tfrac{1}{3}\Xi^{\Delta}_u){\rm Tr}(\hat{\varepsilon})-\tfrac{1}{3}\Xi^{\Delta}_u(\varepsilon_\perp-\varepsilon_\parallel) ,\\
\delta E_c(L)&=\Xi^{L}_d{\rm Tr}(\hat{\varepsilon}) .
\end{aligned} \tag{29}$$

2. Valence-band deformation potentials

For the triply degenerate $\Gamma^{25'}$ valence-band states that transform as $|yz\rangle$, $|zx\rangle$, and $|xy\rangle$, the Hamiltonian matrix Eq. (25) is diagonal and takes the form[30]

$$H^{\varepsilon}_v(\Gamma)=\begin{bmatrix} l\varepsilon_\parallel+m(\varepsilon_\parallel+\varepsilon_\perp) & 0 & 0\\ 0 & l\varepsilon_\parallel+m(\varepsilon_\parallel+\varepsilon_\perp) & 0\\ 0 & 0 & l\varepsilon_\perp+2m\varepsilon_\parallel\end{bmatrix} . \tag{30}$$

With the Hamiltonian Eq. (19) and using Eq. (28), the deformation potentials l, m, and n are

$$\begin{aligned}
l&=\left\langle yz\left|-\frac{p_x^2}{m}+V_{xx}\right|yz\right\rangle ,\\
m&=\left\langle yz\left|-\frac{p_y^2}{m}+V_{yy}\right|yz\right\rangle ,\\
n&=\langle yz\left|-\frac{p_xp_y}{m}+V_{xy}\right|zx\right\rangle .
\end{aligned} \tag{31}$$

We have calculated these quantities employing Eqs. (28) and using the same Bloch functions as in Eq. (23).

IV. RESULTS

In this section, we summarize our findings for various band gaps, masses, and deformation potentials for (100)-strained $Si_{1-x}Ge_x$ bulk alloys. The results in this section are based on the full diagonalization of the strained, relativistic Hamiltonian Eq. (1). As discussed in the Introduction, the strain is thought of as originating from the lattice matched growth of a $Si_{1-x}Ge_x$ alloy on top of a thick, unstrained substrate that consists of a bulk $Si_{1-y}Ge_y$ alloy. In order to clearly distinguish between these alloys, we will refer to the strained $Si_{1-x}Ge_x$ alloy with the lateral lattice constant $a_\parallel(x)=a_0(y)$ and a vertical lattice constant given by Eq. (9) as the "active" material. The unstrained $Si_{1-y}Ge_y$ alloy will be called substrate. The gaps and masses reported in this section always refer to the active material.

A. Energy gaps

Figure 1 depicts the calculated minimal-energy gap, relative to the top of the valence band, as a function of the active alloy composition x and the substrate composition y. The lines bounding the graph in the x direction represent strained alloys grown on a pure Si ($y=0$) or pure Ge ($y=1$) buffer, whereas those along the y direction correspond to strained Si ($x=0$) or strained Ge ($x=1$), grown on a thick alloy buffer. The gap is largest in unstrained Si ($x=0$ and $y=0$) and smallest in fully strained Si ($x=0$ and $y=1$). It remains Si-like for most compositions and strains and is Ge-like only for weakly strained alloys with high Ge content. In the latter case, the conduction-band minimum lies at the N point (i.e., the L point for pure Ge). For a Si-like gap, on the other hand, it lies on the twofold $\Delta_\perp$ axis as long as the active

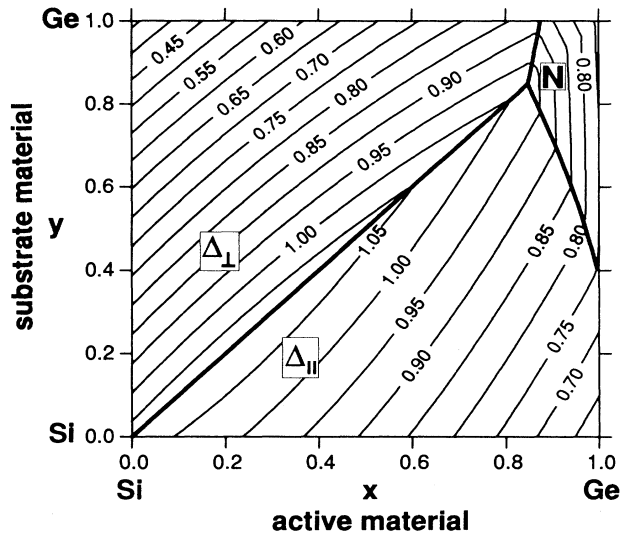

FIG. 1. Calculated fundamental gaps in eV of (100)-strained $Si_{1-x}Ge_x$ alloys (active material) grown pseudomorphically on unstrained $Si_{1-y}Ge_y$ alloys (substrate material).

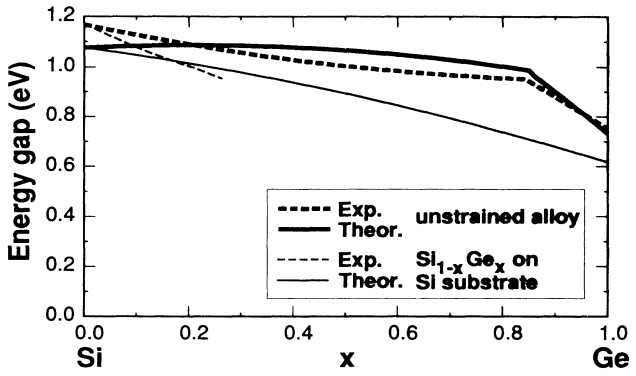

FIG. 2. Comparison of theoretical (full lines) and experimental (dashed lines) data for the fundamental gap in unstrained $Si_{1-x}Ge_x$ alloys and for pure Si grown on a $Si_{1-x}Ge_x$ substrate. The experimental value for the bulk alloy (thick dashed line) are taken from Ref. 34. The strained alloy data are from Ref. 35 for $0<x<0.22$ and from Ref. 36 for $0.22<x<0.26$ (thin dashed line).

alloy has a higher Si content than the substrate, and on the fourfold $\Delta_\parallel$ axis otherwise, in accordance with previous results.[14–16] For high field transport calculations, not only the minimum gap but also higher conduction-band minima need to be known. We have therefore parametrized the energy gaps as

$$E_{\rm gap}(x,y)=[1,(x-y),(x-y)^2]\cdot\mathbf{G}\cdot\begin{bmatrix}1\\(x+y)\\(x+y)^2\end{bmatrix}, \quad (32)$$

where $\mathbf{G}$ is a 3×3 matrix. Each element of this matrix is represented as

$$G_{ij}=G_{ij}^{<}\Theta(y-x)+G_{ij}^{>}\Theta(x-y)\ . \quad (33)$$

These elements are given in Table II for the energy minima on the Δ axes and on N. In strained Ge, i.e., for $x=1$, the conduction-band minimum at the Γ point can also play a role in electronic transport. The energy gap (in eV) of this band edge may be represented in the form $E^{\Gamma}_{\rm gap}(x=1)=g_1+g_2y+g_3y^2$ with $g_1=1.130\,98$, $g_2=-0.101\,06$, and $g_3=-0.139\,19$.

Table II reveals that the linear deformation potential theory widely employed in the analysis of data in SiGe systems does not adequately predict the energy gap of $Si_{1-x}Ge_x$ alloys for all degrees of strain. This is particularly true at the N point where $\mathbf{G}$ contains large quadratic components.

In Fig. 2, we compare the calculated gaps of unstrained $Si_{1-x}Ge_x$ alloys and of strained $Si_{1-x}Ge_x$ alloys on a Si substrate (i.e., with $y=0$) with the experimental data. The overall agreement is quite good even though some shortcomings of the present theory are also visible. First, the calculations yield a fundamental gap of 1.07 eV in pure Si (in accord with the previously calculated[25] value of 1.05 eV) whereas the standard experimental value is

TABLE II. Parametrized energy gaps (in eV) of the three lowest conduction bands in (100)-strained $Si_{1-x}Ge_x$:$Si_{1-y}Ge_y$ alloys in terms of the 3×3 matrix G as defined by Eq. (32). The first column gives the band edge to which the gap refers. Each table entry contains the Cartesian components $G_{ij}^{<}$ and $G_{ij}^{>}$, as defined by Eq. (33).

Gap	j / i	$G_{ij}^{<}$ 1	2	3	$G_{ij}^{>}$ 1	2	3
$\Delta_\perp$	1	1.077 900	0.806 320	0.052 413	1.078 100	0.253 620	0.030 001
	2	0.052 736	−0.170 260	−0.170 560	0.047 577	0.072 361	−0.120 630
	3	−0.061 851	0.036 626	0.058 282	−0.059 023	−0.043 058	0.056 297
$\Delta_\parallel$	1	1.078 000	0.195 980	0.029 780	1.077 500	−0.346 010	0.001 446
	2	0.052 405	−0.271 220	−0.154 490	0.048 883	−0.048 859	−0.076 355
	3	−0.061 595	0.051 422	0.058 774	0.059 722	−0.018 944	0.039 134
N	1	2.185 300	−0.016 767	−0.114 550	2.183 200	−0.648 110	−0.114 770
	2	−0.604 800	−0.363 530	−0.286 170	−0.603 940	0.012 404	−0.116 090
	3	−0.059 545	0.106 320	0.137 330	−0.059 809	−0.038 687	0.067 260

1.17 eV at 4 K.[34,35,37] In Ge, on the other hand, the calculated gap agrees very well with experiment. Second, the present model does not reproduce the bowing of the energy gap as a function of x in the unstrained alloys. This bowing is known to be an effect caused by disorder and is not captured by the virtual crystal approximation which is employed in this paper.[38]

B. Effective masses

Figure 3 compares the calculated with the experimental values of the effective longitudinal and transverse masses of the Δ and L minima for unstrained SiGe alloys. Experimental results for masses in unstrained alloys are, to our knowledge, only known for the pure materials. The agreement for these cases is seen to be excellent. It is plausible that the masses of a given minimum vary only weakly with the alloy compositions, but a significant change in the effective mass of the absolute conduction-band minimum occurs of course when the L minimum sinks energetically below the Δ minimum. In addition, we have computed the effective mass associated with the band minimum at $\mathbf{k}=0$ in bulk Ge and find a value of 0.0478. The experimental values for this mass lie between 0.0387 and 0.042.[37]

For transport applications, it is particularly useful to know the conductivity mass since the mobility is inversely proportional to this mass. Figure 4(a) shows the parallel and Fig. 4(b) the perpendicular conductivity mass associated with the lowest conduction-band minimum for all degrees of alloying and strain. The smallest conductivity mass is seen to occur for a Ge-like gap when the minimum lies at N. Discontinuities in the masses occur between the areas of different location of the conduction-band minimum, due to the strict application of the definition Eq. (11). In reality, of course, the finite temperature causes *all* energetically close lying minima to contribute to the conduction and thus smoothes out these discontinuities.

For strained Si grown on $Si_{1-y}Ge_y$ alloys [this corresponds to the left ordinate in Fig. 4(a)], the mass $m_{\parallel}^{c}=m_t$ is predicted to increase slightly with strain relative to the bulk Si value. It turns out that this is in excellent agreement with recent cyclotron resonance data for Si on $Si_{0.7}Ge_{0.3}$, which indeed indicate such a minor increase in the transverse effective mass.[42]

Table III contains parametrized transverse (m_t) and longitudinal (m_l) effective masses associated with the three band minima as a function of alloy composition x and y in the form

$$m^*(x,y)=[1,(x-y),(x-y)^2]\cdot\mathbf{W}\cdot\begin{bmatrix}1\\(x+y)\end{bmatrix}. \quad (34)$$

Figure 5 shows the calculated valence-band parameters L, M, and N with varying Ge content x of the alloy. For the pure elements, the predicted values agree quite well with experiment. For Si in particular, the present

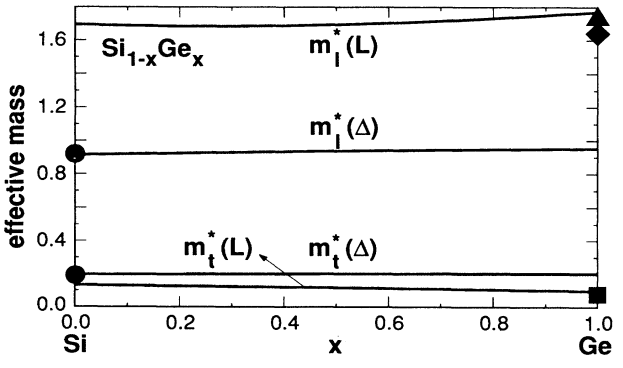

FIG. 3. Calculated longitudinal and transverse effective masses (in units of the electron mass) at the L and Δ minima in unstrained $Si_{1-x}Ge_x$ alloys. For the pure materials, experimental data have been included for comparison. The Si values are taken from Ref. 39 (circles) and for Ge from Ref. 39 (triangle), 40 (caret), and 41 (square).

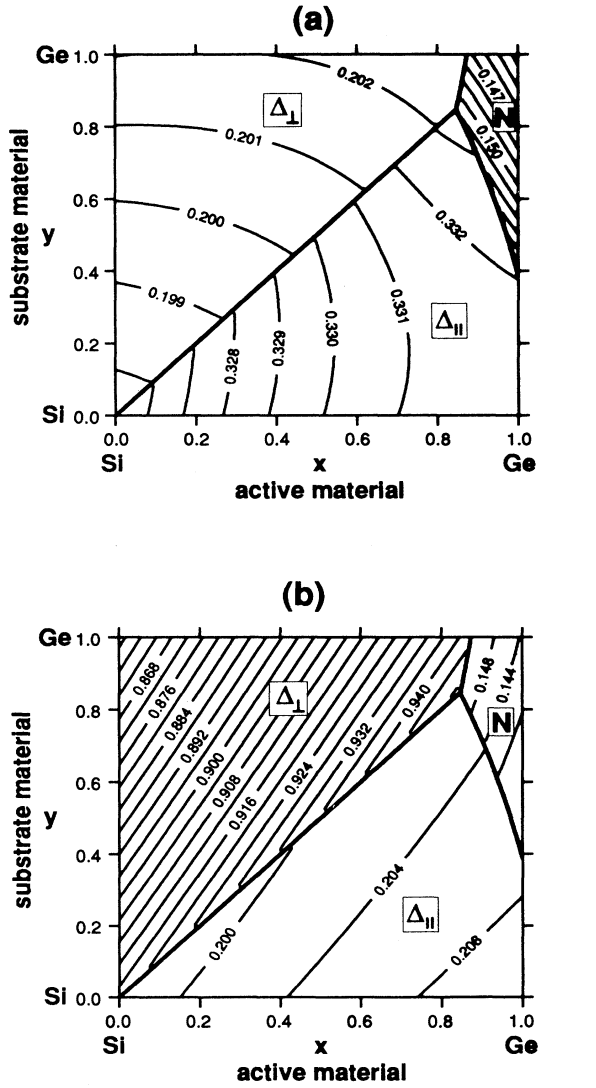

FIG. 4. Calculated (a) parallel and (b) perpendicular conductivity mass (in units of the electron mass) in a strained $Si_{1-x}Ge_x$ alloy (active material) grown on a $Si_{1-y}Ge_y$ substrate.

TABLE III. Parametrized effective transverse and longitudinal conduction-band masses (in units of the electron mass) in (100)-strained $Si_{1-x}Ge_x$:$Si_{1-y}Ge_y$ alloys in terms of the 3×2 matrix **W** as defined by Eq. (34). The first column gives the band edge to which the mass tensor refers. Each table entry contains the cartesian components W_{ij}.

Gap	Mass	W_{11}	W_{21}	W_{31}	W_{12}	W_{22}	W_{32}
$\Delta_\perp$	m_l^*	0.918 000 0	0.082 821 0	−0.004 386 2	0.018 728 0	−0.000 393 0	0.004 424 9
	m_{t1}^*	0.197 490 0	−0.001 154 3	0.000 976 7	0.002 828 1	0.000 799 2	0.000 375 0
	m_{t2}^*	0.197 490 0	−0.001 154 3	0.000 976 7	0.002 828 1	0.000 799 2	0.000 375 0
$\Delta_\parallel$	m_l^*	0.917 930 0	0.015 733 0	0.000 530 7	0.018 794 0	−0.008 054 1	−0.000 888 7
	m_{t1}^*	0.197 480 0	0.004 987 7	−0.000 733 6	0.002 842 1	−0.003 482 9	0.000 153 8
	m_{t2}^*	0.197 440 0	0.014 813 0	−0.001 250 0	0.002 860 5	−0.003 466 6	0.000 128 8
N	m_l^*	1.659 200 0	0.054 035 0	−0.184 200 0	0.041 246 0	0.052 626 0	0.033 581 0
	m_{t1}^*	0.133 190 0	−0.054 784 0	0.026 876 0	−0.017 388 0	0.016 052 0	−0.012 321 0
	m_{t2}^*	0.133 060 0	0.025 237 0	0.002 931 4	−0.017 356 0	−0.014 549 0	−0.005 153 4

theoretical and the experiment[37] values for L, M, and N are −6.69 (−6.64), −4.62 (−4.60), and −8.56 (−8.68), respectively, with the experimental values given in parenthesis. These theoretical results agree marginally better with experiment than the previously calculated values of Chelikowski and Cohen,[32] who found −6.85, −4.23, and −8.41, respectively, but inconsistently neglected the correction terms in Eq. (21) proportional to $V_{\rm nloc}$ and used a slightly different pseudopotential.

Noticeably, the present theory predicts the $\mathbf{k}\cdot\mathbf{p}$ parameter M to vary practically linearly with x, whereas L and N are predicted to show a highly nonlinear variation. We cannot, of course, rule out that this result is an artifact of the virtual-crystal approximation. We note, however, that the known failure of this approximation to fully reproduce the bowing of the conduction band (see Fig. 2) cannot account for such a dramatic nonlinearity. If we assume that $m^* \propto 1/E_{\rm gap}$, the bowing in the conduction band of $Si_{1-x}Ge_x$ gives a much weaker nonlinearity for the parameters L and N.

We found the following expression to give an excellent fit to the calculated values; P stands equally for L, M, or N.

$$P(x)=P(0)+\alpha\ln(1-Sx^\beta)\ ,$$
$$S=1-\exp\{[P(1)-P(0)]/\alpha\}\ . \tag{35}$$

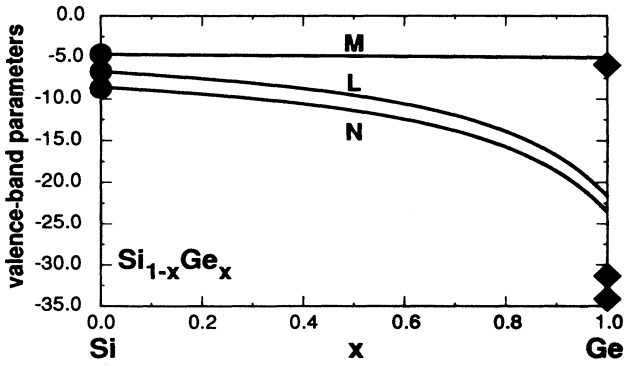

FIG. 5. Calculated valence-band parameters in an unstrained $Si_{1-x}Ge_x$ alloy. For pure Si (Ref. 43) and Ge (Ref. 44) the experimental results are shown for comparison. Units are $\hbar^2/(2m)$.

The parameters are $\alpha=6.7064$, $\beta=1.35$, $L(0)=-6.69$, $M(0)=-4.62$, $N(0)=-8.56$, $L(1)=-21.65$, $M(1)=-5.02$, and $N(1)=-23.48$.

C. Deformation potentials

Employing the pseudopotential expressions given in Sec. III C, we have calculated several interband deformation potentials of unstrained $Si_{1-x}Ge_x$ alloys. Note that these quantities do not depend on the average crystal potential, which is somewhat uncertain in the empirical pseudopotential method.

Figures 6(a)–6(d) summarize the calculations and also show several experimental results for Si and Ge. Unfortunately, the available data scatter too much to provide a stringent test for the theory. Previous calculations are summarized in Table IV and also reflect the appreciable uncertainties in these quantities.

In order to evaluate the accuracy of linear deformation potential theory, it is instructive to compare its predictions with the full calculations that include strain and spin-orbit effects to all orders (given in Sec. IV A). In strained Si, for example, the conduction-band minimum lies on the $\Delta_\perp$ axis for any substrate $Si_{1-y}Ge_y$ composition y. To first order in the strain, it changes according to the relation

$$\delta E_{\rm gap}(\hat{\varepsilon};{\rm Si})=(\Xi_d^\Delta+\tfrac{1}{3}\Xi_u^\Delta-a){\rm Tr}(\hat{\varepsilon})+(\tfrac{2}{3}\Xi_u^\Delta-2b)\varepsilon_{\rm ax}\ , \tag{36}$$

where $a=(l+2m)/3$ and $b=(l-m)/3$ contain the valence-band deformation potentials and $\varepsilon_{\rm ax}=(a_\perp-a_\parallel)/a_0$. For maximum strain ($y=1$), this equation gives a gap of 0.31 eV. This is in good agreement with the gap of 0.34 eV that is predicted by the full calculation (Sec. IV A).

In highly strained Ge with substrate composition $y<0.4$, the conduction-band minimum lies on the $\Delta_\parallel$ axis and changes according to

$$\delta E_{\rm gap}^\Delta(\hat{\varepsilon};{\rm Ge})=(\Xi_d^\Delta+\tfrac{1}{3}\Xi_u^\Delta-a){\rm Tr}(\hat{\varepsilon})-(\tfrac{1}{3}\Xi_u^\Delta-b)\varepsilon_{\rm ax}\ . \tag{37}$$

For $y=0$, this equation yields $E_{\rm gap}=0.65$ eV whereas

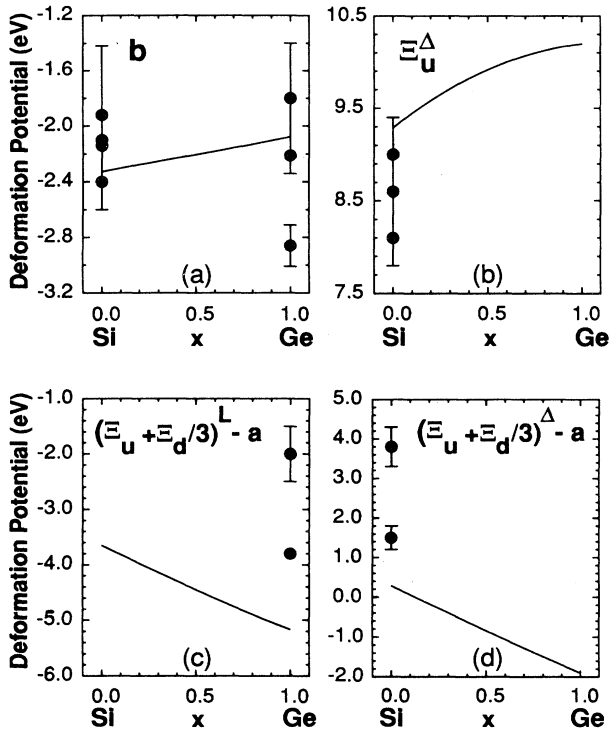

FIG. 6. Deformation potentials in $Si_{1-x}Ge_x$ alloys from the present calculations pertaining to band shifts and splittings under biaxial (100) strain. The experimental results for the pure materials are also indicated. (a) References 45–48 for Si and Refs. 44, 48, and 49 for Ge; (b) Refs. 45, 47, 48, and 50; (c) Refs. 48 and 51; and (d) Refs. 47 and 48.

the complete theory gives 0.62 eV. For other combinations of active material and substrate, however, the higher-order strain effects included in the full calculation have somewhat larger effects. This is particularly the case in the alloy regime near Ge, as discussed in Sec. IV A.

TABLE IV. Calculated strain deformation potentials (in eV) in bulk Si and Ge.

	Deformation potential	Present work	Previous theories
Si	b	−2.33	−2.18,[a] −2.35,[b] −3.0[c]
	Ξ_u^Δ	9.29	8.0,[a] 9.16[b]
	$(\Xi_d+\Xi_u/3)^\Delta-a$	0.29	1.2,[a] 1.72,[b] 1.6[d]
	$(\Xi_d+\Xi_u/3)^L-a$	−3.65	−4.3,[a] −3.12,[b] −3.8[d]
Ge	b	−2.08	−2.30,[a] −2.55,[b] −3.1[c]
	Ξ_u^Δ	10.20	8.9,[a] 9.42[b]
	$(\Xi_d+\Xi_u/3)^\Delta-a$	−1.90	0.32,[a] 1.31,[b] 1.1[d]
	$(\Xi_d+\Xi_u/3)^L-a$	−5.17	−4.2,[a] −2.78,[b] −3.5[d]

[a]Reference 52.
[b]Reference 8.
[c]Reference 53.
[d]Reference 54.

D. Energy-band offsets

An exceedingly relevant electronic property for both transport and optical device applications is the band alignments across heterointerfaces. Particularly optoelectronic applications require both electrons and holes to be confined within the active layer, i.e., a type-I alignment of the band edges with $\Delta E_c = E_c(Si_{1-x}Ge_x) - E_c(Si_{1-y}Ge_y) < 0$ and $\Delta E_v = E_v(Si_{1-x}Ge_x) - E_v(Si_{1-y}Ge_y) > 0$.

The experimental values for the band offsets are still somewhat uncertain. Early measurements[55,56] indicated rather small valence-band offsets between Si and Ge of $\Delta E_v = 0.4 \pm 0.1$ eV, but did not account for the effects of strain on the valence-band edge. This was done only recently by Schwartz *et al.*,[57] who supplemented their photoemission data with deformation potential calculations and found a valence-band offset of $\Delta E_v(x=1,y=0) = 0.74 \pm 0.13$ eV for strained Ge on cubic Si(100) and $\Delta E_v(x=0,y=1) = -0.17 \pm 0.13$ eV for Si on Ge(100). These values are in excellent agreement with recent calculations of Colombo, Resta, and Baroni,[9] who predict $\Delta E_v(x=0,y=1) = 0.74$ eV and $\Delta E_v(x=1,y=0) = -0.21$ eV.

We have made use of our calculations to give a comprehensive survey of the valence- and conduction-band offsets at the interface between a cubic and a strained layer of SiGe alloys of differing Ge content.

The empirical pseudopotential method by itself is not suited to produce energy levels on an absolute scale reliably but gives only relative positions of the bands. Once we know, however, the alignment of just one reference point on the energy scale at both sides of the interface, the alignment of the individual bands can be derived from the present calculations. In Ref. 9, the offset of the *average* energy of the uppermost three valence bands has been calculated for a strained Si/Ge (100) interface with *ab initio* methods. The findings there indicate, as did the earlier calculations of Van de Walle and Martin,[8] that the offset is nearly independent of the strain conditions, apart from a weak, linear variation of the offset with the lattice constant parallel to the interface. To obtain values for the offset for all situations considered in the present work, we assume furthermore the offset to vary linearly with alloying, in agreement with Ref. 8, and thus arrive at the formula

$$\Delta V_{av} = (0.47 - 0.06y)(x - y) \tag{38}$$

for the offset between the average of the valence-band edge in a strained $Si_{1-x}Ge_x$ layer and an unstrained $Si_{1-y}Ge_y$ layer. (Positive values refer to higher energies in the strained layer.)

By employing the complete Hamiltonian Eq. (1) for both sides of the interface and using Eq. (38) to set the band alignment, we get the data for Figs. 7(a) and 7(b) that depict the valence- and conduction-band offsets. These figures reveal that $Si_{1-x}Ge_x$:$Si_{1-y}Ge_y$ is a type-II heterostructure for most alloy compositions: the offsets have the same sign for conduction and valence bands. In accordance with the previous estimates of Ref. 15, we find very small conduction-band offsets for $Si_{1-x}Ge_x$ on

Si substrate for $x < 0.3$. Whereas People and Bean[7] suggested a marginal type-I heterostructure for these compositions, the present calculations always give a marginal type-II alignment if the substrate is unstrained Si. This is also in agreement with the conclusions of Ref. 15.

Importantly, however, the present theory does predict a range of compositions where the lattice-matched alloys manifestly show type-I band alignment: Figures 7(a) and 7(b) show the energy gap of weakly strained Ge-rich active material with $0.75 \leq x \leq 1$ to fall within the wider gap of a Ge-rich substrate with $0.6 \leq y \leq 1$. Especially for (100)-strained Ge with a substrate composition of 85% Ge, the conduction- and valence-band offset is -0.13 and 0.10 eV, respectively, allowing a weak confinement of both electrons and holes in the active layer.

In Figs. 8 and 9, we provide a survey of the band offsets and relative energy gaps in the pure strained materials. The depicted combinations of active material and substrate correspond to the bounding vertical lines in Figs. 7(a) and 7(b). The series of pictures in Figs. 8 and 9 gives an overview of the band-edge states in the active and substrate materials. The Ge content is indicated by shades of grey and ranges from light (pure Si) to dark grey (pure Ge). The left part in each picture shows the symmetry and energetic position of the lowest and second lowest conduction-band minimum, and the heavy-hole (hh), light-hole (lh), and split-off (so) valence band at the Γ point. The right-hand part in each figure depicts the conduction- and valence-band-edge state in the unstrained substrate. The full circles indicate the funda-

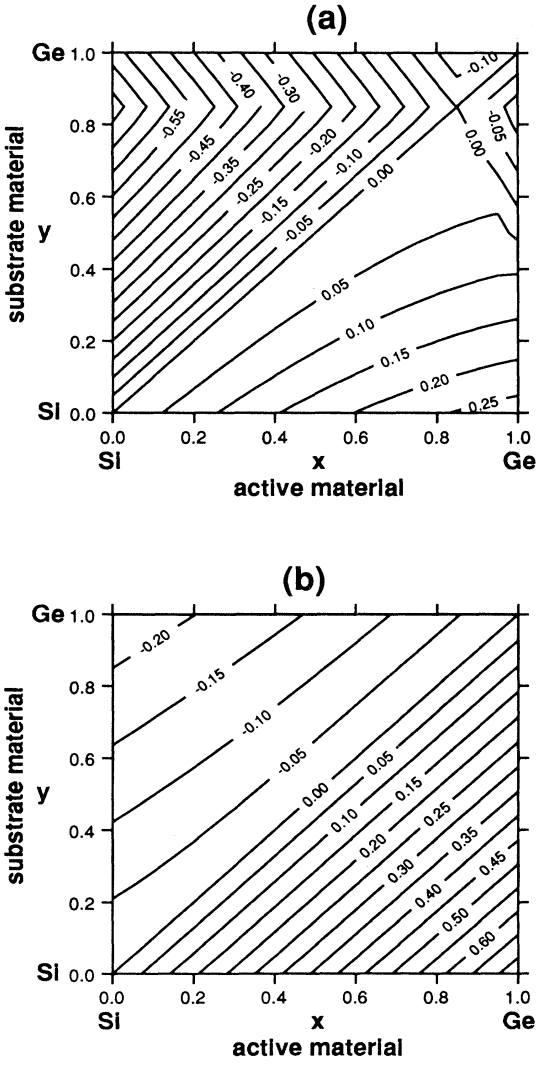

FIG. 7. (a) Conduction-band offsets $E_c(x) - E_c(y)$ and (b) valence-band offsets $E_v(x) - E_v(y)$ in eV at the interface of a lattice matched (100)-strained $Si_{1-x}Ge_x$ bulk alloy and a cubic $Si_{1-y}Ge_y$ bulk substrate, derived from the present calculations.

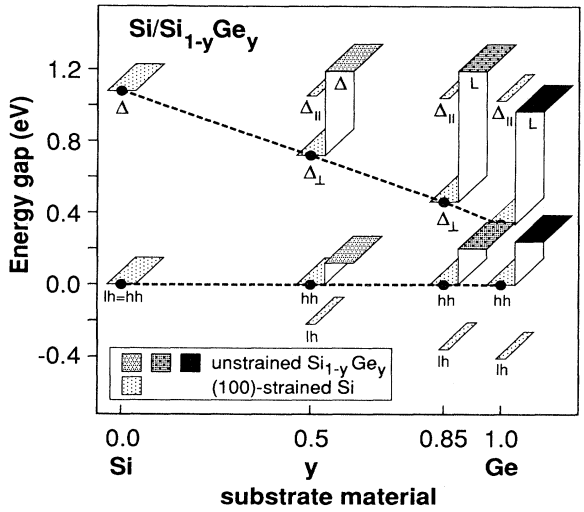

FIG. 8. Symmetry and relative energetic positions of the band-edge states in (100)-strained lattice matched Si (left part of each depicted heterostructure) and in unstrained substrates (right part). The fundamental band gap in strained Si is indicated by full circles, which are interconnected to guide the eye. The second lowest conduction-band minima and the top valence-band states in Si are also indicated. The grey shades in the pictures indicate the Ge content.

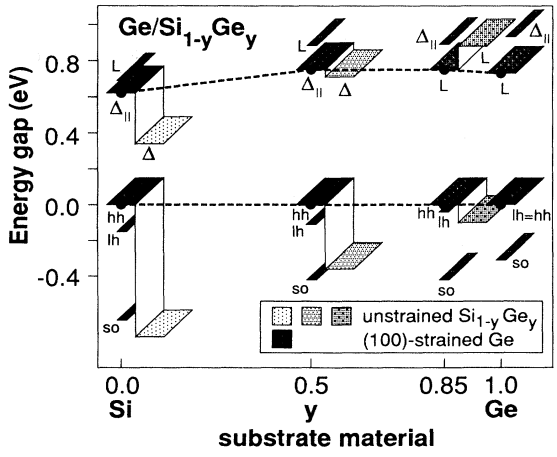

FIG. 9. Same as Fig. 8, but for Ge as the active material.

mental band gap in the active material; they have been interconnected by dashed lines only to guide the eye. In Fig. 8, the conduction- and valence-band edge in strained Si is seen to lie always lower than in the substrate. This corresponds to a type-II alignment. In the case of Ge (Fig. 9), the band minima lie generally higher than in the substrate. However, the conduction- and valence-band edges of strained Ge lie *within* the gap of the substrate for $Si_{1-y}Ge_y$ alloys with $y \sim 0.85$, giving a type-I interface.

V. SUMMARY AND CONCLUSION

We have systematically investigated the electronic properties of (100)-strained $Si_{1-x}Ge_x$:$Si_{1-y}Ge_y$ alloys that are relevant for device applications, namely effective masses, band gaps, deformation potentials, and band offsets. The main results of this paper can be deduced from Figs. 8 and 9 that give a survey of the conduction- and valence-band states in (100)-strained Si and Ge near the fundamental gap, and the band offsets between the strained and unstrained lattice-matched materials.

Noticeably, Ge is predicted to possess a type-I heterointerface with Ge-rich $Si_{1-y}Ge_y$ substrate material. This implies that both types of carriers can be simultaneously confined in the active Ge layer, in contrast to any Si-rich combination of active layer and substrate. Both this fact and the small effective masses in Ge-rich material indicate that weakly strained Ge-rich SiGe layers possess very promising properties for both electronic and optical applications.

ACKNOWLEDGMENTS

Many helpful and illuminating discussions with G. Abstreiter, who initiated this work, are gratefully acknowledged. This work was supported by the Deutsche Forschungsgemeinschaft and by the Siemens Corporation.

[1]S. C. Jain, J. R. Willis, and R. Bullough, Adv. Phys. **39**, 127 (1990).

[2]E. Kasper and F. Schäffler, in *Strained Layer Superlattices: Materials Science and Technology,* Vol. 33 of *Semiconductors and Semimetals,* edited by T. P. Pearsall (Academic, New York, 1991), p. 223.

[3]G. Abstreiter, J. Brunner, F. Meier, U. Menczigar, J. Nützel, R. Schorer, and D. Többen, *Proceedings of the 21st International Conference on the Physics of Semiconductors,* edited by Ping Jiang and Hou-Zhi Zheng (World Scientific, Singapore, 1992), Vol. 1, p. 827.

[4]F. Schäffler, D. Többen, H.-J. Herzog, G. Abstreiter, and B. Holländer, Semicond. Sci. Technol. **7**, 260 (1992).

[5]D. Többen, F. Schäffler, A. Zrenner, and G. Abstreiter, Phys. Rev. B **46**, 4344 (1992).

[6]J. C. Sturm, H. Manoharan, L. C. Lenchyshyn, M. L. W. Thewalt, N. L. Rowell, J.-P. Noël, and D. C. Houghton, Phys. Rev. Lett. **66**, 1362 (1991).

[7]R. People and J. C. Bean, Appl. Phys. Lett. **48**, 538 (1986).

[8]C. G. Van de Walle and R. M. Martin, Phys. Rev. B **34**, 5621 (1986).

[9]L. Colombo, R. Resta, and S. Baroni, Phys. Rev. B **44**, 5572 (1991).

[10]S. Sathpathy, R. M. Martin, and C. G. Van de Walle, Phys. Rev. B **38**, 13 237 (1988).

[11]S. Froyen, D. M. Wood, and A. Zunger, Phys. Rev. B **37**, 6893 (1988).

[12]U. Schmid, J. Humlíček, F. Lukeš, M. Cardona, H. Presting, H. Kibbel, E. Kasper, K. Eberl, W. Wegscheider, and G. Abstreiter, Phys. Rev. B **45**, 6793 (1992).

[13]K. B. Wong, M. Jaros, I. Morrison, and J. P. Hagon, Phys. Rev. Lett. **6**, 2221 (1988).

[14]G. Abstreiter, H. Brugger, T. Wolf, H. Jorke, and H.-J. Herzog, Phys. Rev. Lett. **54**, 2441 (1985).

[15]Ch. Zeller and G. Abstreiter, Phys. Rev. B **64**, 137 (1986).

[16]R. People, Phys. Rev. B **32**, 1405 (1985).

[17]Y. Rajakarunanayake and T. C. McGill, Phys. Rev. B **40**, 3051 (1989).

[18]J. M. Hinckley and J. Singh, Phys. Rev. B **41**, 2912 (1990).

[19]Q. M. Ma, K. L. Wang, and J. N. Schulman, Phys. Rev. B **47**, 1936 (1993); Zhi-Zong Xu, *ibid.* **47**, 3642 (1993).

[20]C. Tserbak, H. M. Polatoglu, and G. Theodoru, Phys. Rev. B **47**, 7104 (1993).

[21]M. Gell, Phys. Rev. B **41**, 7611 (1990).

[22]F. Bechstedt, Adv. Solid State Phys. **32**, 161 (1992).

[23]M. S. Hybertsen and S. G. Louie, Phys. Rev. B **37**, 2733 (1988).

[24]R. Hott, Phys. Rev. B **44**, 1057 (1991).

[25]J. R. Chelikowsky and M. L. Cohen, Phys. Rev. B **14**, 556 (1976).

[26]W. Pötz and P. Vogl, Phys. Rev. B **24**, 2025 (1981).

[27]S. Bloom and T. K. Bergstresser, Solid State Commun. **6**, 465 (1970); Phys. Status Solidi **42**, 191 (1970).

[28]E. Anastassakis, in *Light Scattering in Semiconductor Structures and Superlattices,* edited by D. J. Lockwood and J. F. Young (Plenum, New York, 1991), p. 173.

[29]J. P. Dismukes, L. Ekstrom, and R. J. Paff, J. Phys. Chem. **68**, 3021 (1964).

[30]G. L. Bir and G. E. Pikus, *Symmetry and Strain-Induced Effects in Semiconductors* (Wiley, New York, 1974).

[31]In the context of the static dielectric function, an analogous extension was given by S. Baroni and R. Resta, Phys. Rev. B **33**, 7017 (1986).

[32]J. R. Chelikowsky and M. L. Cohen, Phys. Rev. B **10**, 5095 (1974).

[33]G. Dresselhaus, A. F. Kip, and C. Kittel, Phys. Rev. **98**, 368 (1955).

[34]J. Weber and M. I. Alonso, Phys. Rev. B **40**, 5683 (1989).

[35]D. Dutartre, G. Brémond, A. Souifi, and T. Benyattou, Phys. Rev. B **44**, 11 525 (1991).

[36]J. Spitzer, K. Thonke, R. Sauer, H. Kibbel, H.-J. Herzog, and E. Kasper, Appl. Phys. Lett. **60**, 1729 (1992).

[37]O. Madelung, in *Tables Numerical Data and Functional Relationships in Science and Technology,* edited by O. Madelung, M. Schulz, and H. Weiss, Landolt-Börnstein, New Series, Group III, Vol. 17, Pt. a (Springer, Heidelberg, 1982).

[38]S. Krishnamurthy, A Sher, and A.-B. Chen, Phys. Rev. B **33**, 1026 (1986).

[39]J. C. Hensel, H. Hasegawa, and M. Nakyama, Phys. Rev. **138**, A225 (1965).
[40]R. N. Dexter, H. J. Zeiger, and B. Lax, Phys. Rev. **104**, 637 (1956).
[41]G. Dresselhaus, A. F. Kip, and C. Kittel, Phys. Rev. **95**, 568 (1954).
[42]G. Schuberth, F. Schäffler, M. Besson, G. Abstreiter, and E. Gornik, Appl. Phys. Lett. **59**, 3318 (1991).
[43]*L*, *M*, and *N* were calculated from the data given for γ_1, γ_2, and γ_3 in Ref. 37.
[44]J. C. Hensel and K. Suzuki, Phys. Rev. B **9**, 4219 (1974).
[45]J. C. Merle, M. Capizzi, P. Fionini, and A. Frova, Phys. Rev. B **17**, 4821 (1978).
[46]H. R. Chandrasekhar, P. Fischer, A. K. Ramdas, and S. Rodriguez, Phys. Rev. B **8**, 3836 (1973).
[47]L. D. Laude, F. H. Pollak, and M. Cardona, Phys. Rev. B **3**, 2623 (1971).
[48]I. Balslev, Phys. Rev. **143**, 636 (1966).
[49]M. Chandrasekhar and F. H. Pollak, Phys. Rev. B **15**, 2127 (1977).
[50]K. Murase, K. Enjouji, and E. Otsuka, J. Phys. Soc. Jpn. **29**, 1248 (1970).
[51]W. Paul and D. M. Warschauer, in *Solids Under Pressure,* edited by W. Paul and D. M. Warschauer (McGraw-Hill, New York, 1963), p. 226.
[52]U. Schmid, N. E. Christensen, and M. Cardona, Solid State Commun. **75**, 39 (1990).
[53]A. Blacha, H. Presting, and M. Cardona, Phys. Status Solidi B **126**, 11 (1984).
[54]K. J. Chang, S. Froyen, and L. Cohen, Solid State Commun. **50**, 105 (1984).
[55]T. F. Kuech, M. Mäenpää, and S. S. Lau, Appl. Phys. Lett. **39**, 245 (1981).
[56]P. H. Mahowald, R. S. List, W. E. Spicer, and P. Pianetta, J. Vac. Sci. Technol. B **3**, 1252 (1985).
[57]G. P. Schwartz, M. S. Hybertsen, J. Bevk, R. G. Nuzzo, J. P. Mannaerts, and G. J. Gualtieri, Phys. Rev. B **39**, 1235 (1989).